INTERNATIONAL JOURNAL FOR NUMERICAL METHODS IN FLUIDS
Int. J. Numer. Meth. Fluids 2003; **41**:1273–1294 (DOI: 10.1002/fld.427)

Numerical method for calculation of the incompressible flow in general curvilinear co-ordinates with double staggered grid

A. Shklyar*,† and A. Arbel

Institute of Agricultural Engineering, Agricultural Research Organization, The Volcani Center, P.O. Box 6, Bet Dagan 50250, Israel

SUMMARY

A solution methodology has been developed for incompressible flow in general curvilinear co-ordinates. Two staggered grids are used to discretize the physical domain. The first grid is a MAC quadrilateral mesh with pressure arranged at the centre and the Cartesian velocity components located at the middle of the sides of the mesh. The second grid is so displaced that its corners correspond to the centre of the first grid. In the second grid the pressure is placed at the corner of the first grid. The discretized mass and momentum conservation equations are derived on a control volume. The two pressure grid functions are coupled explicitly through the boundary conditions and implicitly through the velocity of the field. The introduction of these two grid functions avoids an averaging of pressure and velocity components when calculating terms that are generated in general curvilinear co-ordinates. The SIMPLE calculation procedure is extended to the present curvilinear co-ordinates with double grids.
Application of the methodology is illustrated by calculation of well-known external and internal problems: viscous flow over a circular cylinder, with Reynolds numbers ranging from 10 to 40, and lid-driven flow in a cavity with inclined walls are examined. The numerical results are in close agreement with experimental results and other numerical data. Copyright © 2003 John Wiley & Sons, Ltd.

KEY WORDS: general curvilinear co-ordinates; incompressible flow

1. INTRODUCTION

The main aim of the present study is to devise and test a technique for calculation of incompressible flow in general co-ordinates. A numerical methodology for calculation of flow is identified by a pattern of interaction procedures involving the physical domain and the conservation equation's discretization, boundary conditions and solver.

This method has been developed around the structure of the conservation equations in general co-ordinates. The gradient term in general co-ordinates (Figure 1) is

$$\varphi_x = (\varphi_\xi y_\eta - \varphi_\eta y_\xi)/J \tag{1}$$

* Correspondence to: A. Shklyar, Institute of Agricultural Engineering, Agricultural Research Organization, The Volcani Center, P.O. Box 6, Bet Dagan 50250, Israel.
† E-mail: shklyar@agri.gov.il

Received 1 August 2000
Revised 21 April 2002

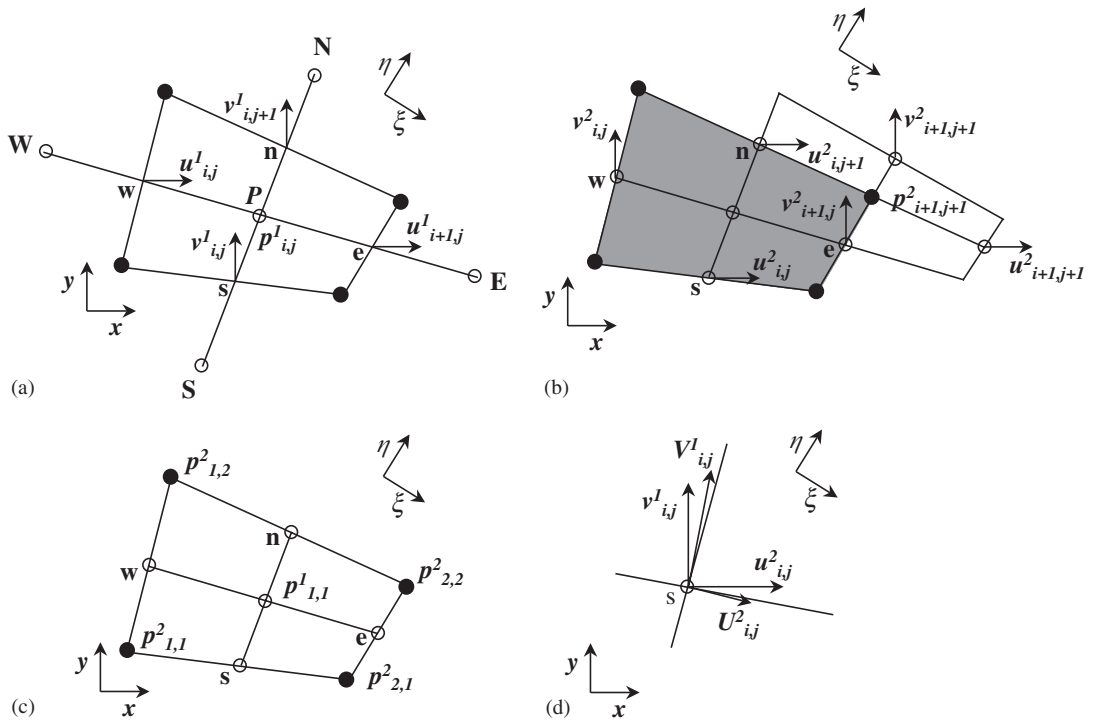

Figure 1. Double set of computational grids: (a) first staggered grid cell; (b) second staggered grid displacement; (c) second pressure cell displacement; (d) a grid for which Cartesian and contravariant velocities are not aligned.

A distinguishing feature of the gradient term in general co-ordinates is the existence of two terms. In developing new methods or algorithms for general co-ordinates it is desirable to retain as many and as much as possible of the advantages and simplicity of existing widely used algorithms for Cartesian co-ordinates (e.g. SIMPLE or SIMPLER, Reference [1]), and there are control volume methods which avoid the calculation of one of these two terms in an explicit form. We will first look more closely at the pressure gradient:

$$p_x = (p_\xi y_\eta - p_\eta y_\xi)/J \tag{2}$$

Use of the staggered grid in general co-ordinates has been described by Shyy *et al.* [2] and by Faghri *et al.* [3]. Since the successive line under-relaxation (SLUR) method was used to solve the system of finite-difference equations by applying the efficient tri-diagonal equation solver, the p_ξ or p_η is dropped. An alternative formulation that was used by Shyy *et al.* [2] also involves putting p_ξ and p_η into the source term. A two-dimensional kidney-shaped channel was used to illustrate the application of the algorithm. The flow pattern in this control case has a main direction, and it is valid to neglect one of the terms in Equation (2).

Alternative ways to exploit all the advantages of the five-point difference equation were presented by Faghri *et al.* [3] who eliminated p_ξ or p_η by averaging neighbouring pressures,

and by Maliska and Raithby [4] who used linear interpolation to account for the non-uniform grid.

Velocity is a second primitive variable; the x component in general co-ordinates, in accordance with Equation (1) is

$$u_x = (u_\xi y_\eta - u_\eta y_\xi)/J \tag{3}$$

Approximation of the velocity in the discretized space presents many problems, in addition to the above equations (as shown by Peyret and Taylor [5]).

The problems of discretization of the physical domain and of the conservation equations are a major focus of interest in the present study.

2. DISCRETIZATION PROCEDURE

2.1. Physical domain discretization

To facilitate the derivation of the finite-difference formulation, the solution domain in the x, y co-ordinate system is first discretized. Peyret and Taylor [5] discussed the effect of the mesh on the numerical solution. A computational procedure was developed by Lien *et al.* [6] (and others whom they cite), on the basis of finite volumes, which are collocated so that all flow variables are stored at one and the same set of nodes. For this collocation arrangement Rhie and Chow [7] proposed a non-linear interpolation scheme for formulating the pressure–velocity coupling form. Thus, we want to use the staggered grid technique, which offers conservation of mass, momentum and kinetic energy in a natural way, and which avoids the decoupling of odd–even points. The staggered grid in general curvilinear co-ordinates has been operated in methodologies described by Shyy *et al.* [2], Faghri *et al.* [3] and Maliska and Raithby [4].

Two grids are used to discretize the physical domain. For the first grid, a MAC [5] staggered grid system is adopted, as shown in Figure 1(a). A grid system is generated numerically or algebraically at the position marked by filled circles. The pressure $p^1_{i,j}$ is arranged at the arithmetic centre of these four circles. The numerical notation of the p^1 is designed so that indexes $(1,1)$ belong to the left bottom mesh of the domain, $p^1_{i,0}$ lies at the bottom and $p^1_{0,j}$ belongs to the left boundary. The Cartesian velocity components $u^1_{i+1,j}$ and $u^1_{i,j}$ are located at the midpoints of the e and w faces of the control volume, and the Cartesian velocity components $v^1_{i,j}$ and $v^1_{i,j+1}$ are located at the midpoints of the s and n faces of the control volume. A typical grid node, P, is enclosed in its cell and surrounded by its neighbours N, S, E, and W. The second grid (Figure 1(b)) is displaced so that the centre of its mesh coincides with the corner of that of the first mesh grid (shaded area) and its corners correspond to the centre of that of the first grid. The pressure $p^2_{i,j}$ in the second grid is placed at the corner of the first mesh. Note that for convenience in numerical coding and the relation between first and second grid indexes, fractional indexes are not used in notations, e.g. $p^2_{1,1}$ belongs to the left bottom corner and $p^2_{2,2}$ to the diagonally opposite corner of the first grid mesh (Figure 1(c)). The Cartesian velocity components $u^2_{i,j}$ and $u^2_{i,j+1}$ are located at the midpoints of the s and n faces of the first grid control volume, and the Cartesian velocity components $v^2_{i+1,j}$ and $v^2_{i,j}$ are located at the midpoints of the e and w faces of the first grid control volume. Thus, two sets of the primitive variables define the physical domain, indexes of the

first velocity component u^1 coincide with those of the second velocity component v^2, that also is valid for u^2 and v^1. For this mesh type, Peyret and Taylor [5] note, 'it would be possible to couple (weakly) the two fields by way of the special technique needed to define the pressure on Γ'.

The transformation from the physical domain to rectangular co-ordinates may be done by conventional methods. The terminology, notation, coefficients and relationships for the geometric metric used here are derived from Thompson [8], and will be explained within their context, as necessary.

2.2. Discretization of the continuity equation

We consider incompressible, steady-state flow. The mass flux, $\rho\mathbf{u}$ is integrated over a control volume in physical space, bounded by lines of constants ξ and η.
($p^1_{i,j}$ is placed in the centre of this volume),

$$\int_S \rho\mathbf{u}\cdot\mathbf{n}\,\mathrm{d}s = 0 \tag{4}$$

Here $\mathbf{u}$ is a velocity vector, written as $\mathbf{u}=[u,v]$, with Cartesian components u,v, and unit vector $\mathbf{n}=[n_x,n_y]$ normal to the surface element $\mathrm{d}s$, S is the enclosing surface of finite volume.

For evaluation of the surface integral, expressions are needed for the surface element $\mathrm{d}s$ and the normal unit vector $\mathbf{n}$. As suggested above, for the quadrilateral mesh, the surface integral may be subdivided into the sum of four surface integrals over the segments $\mathrm{d}s_e$, $\mathrm{d}s_w$, $\mathrm{d}s_s$, $\mathrm{d}s_n$, respectively.

Only the integral over the surface $\mathrm{d}s_e$ will be evaluated here, as an example. In the general form [8]

$$\mathrm{d}s_e = g_{22}^{1/2}\,\mathrm{d}\eta = h_\eta\,\mathrm{d}\eta, \quad \mathbf{n} = \frac{1}{h_\eta}(\mathbf{e}_x y_\eta - \mathbf{e}_y x_\eta) \tag{5}$$

where $\mathbf{e}_x$, $\mathbf{e}_y$ are the Cartesian unit vectors, $\mathbf{g}$ is the matrix transformation

$$\begin{aligned} g_{11} &= x_\xi^2 + y_\xi^2, \quad g_{12} = g_{21} = x_\xi x_\eta + y_\xi y_\eta, \quad g_{22} = x_\eta^2 + y_\eta^2, \\ J &= x_\xi y_\eta - x_\eta y_\xi, \quad h_\eta = g_{22}^{1/2} \end{aligned} \tag{6}$$

The integrations are performed by regarding all values as constant over each face:

$$\rho U^1_{i+1,j} - \rho U^1_{i,j} + \rho V^1_{i,j+1} - \rho V^1_{i,j} = 0 \tag{7}$$

The U,V in this equation, are the contravariant velocity components, written without metric normalization (as shown in Figure 1(d), the Cartesian velocities (u,v) are not aligned with these contravariant velocity components), where $\mathrm{d}\eta = \mathrm{d}\xi$ without loss of generality

$$U^1_{i,j} = u^1_{i,j} y_\eta - v^2_{i,j} x_\eta \tag{8}$$

$$V^1_{i,j} = v^1_{i,j} x_\xi - u^2_{i,j} y_\xi \tag{9}$$

Under interpolation of Equation (4), ρU and ρV are the mass fluxes across the cell surfaces given by η and ξ lines, respectively. On the 'one-staggered-grid approximation' the contravariant velocity component is calculated in the form

$$U^1_{i,j} = u^1_{i,j} y_\eta - v_{i,j} x_\eta \tag{10}$$

where $v_{i,j}$ is approximated from the 'one grid'. Thus contravariant velocity components of the first grid are linked to the second grid through Equations (8) and (9).

For the second pressure cell (i.e. for a control volume with midpoint $p^2_{i+1,j+1}$) the discrete mass balance is

$$\rho U^2_{i+1,j+1} - \rho U^2_{i,j+1} + \rho V^2_{i+1,j+1} - \rho V^2_{i+1,j} = 0 \tag{11}$$

$$U^2_{i,j} = u^2_{i,j} y_\eta - v^1_{i,j} x_\eta \tag{12}$$

$$V^2_{i,j} = v^2_{i,j} x_\xi - u^1_{i,j} y_\xi \tag{13}$$

Note, that indexes of the contravariant velocity components U^1, V^2 coincide at the same point, and this is also valid for U^2, V^1.

2.3. Evaluation of metrics

Before deriving the discrete analogue of the momentum equation, some comments about the evaluation of the metric and of the metric derivatives are appropriate.

Shyy *et al.* [2] used two methods of evaluating the metric derivatives. In the first approach, if x_η (at the midpoint of the e surface of the control volume for p^1) (Figure 1(a)) is to be evaluated, method I calculates it by taking the quotient of the distance in the y direction between the two endpoints of the e surface, and the distance in the η direction between the same two points. Method II calculates the midpoint by interpolating linearly between the values already calculated at points P and E. The metric derivatives at point P are evaluated by central differencing, based on the geometric relations of the four endpoints that define the control volume. In the algorithm presented by Shyy *et al.* [2], method I is more accurate than method II in fulfilling the physical conservation laws.

The problems of the metric evaluation were examined thoroughly by Thompson [8], and we follow one basic rule: 'never average the metric coefficients'.

We define

$$x_\eta|_e = (x_{i+1,j+1} - x_{i+1,j})/\mathrm{d}\eta \tag{14}$$

$$x_\xi|_e = (x_{i+2,j} - x_{i,j} + x_{i+2,j+1} - x_{i,j+1})/4\,\mathrm{d}\xi \tag{15}$$

By this elementary geometrical reasoning, the value of the derivative (Equation (14)) may be used not only for e point but for P and E points as well

$$x_\xi|_P = x_\xi|_e = x_\xi|_E \tag{16}$$

Thus, the values $x_\xi|_e$ and $x_\eta|_e$ are assigned to all control volumes with midpoint u^1. This definition of the evaluation of the metric is fully symmetrical and descriptive with reference to double-discretized pressure fields.

Symmetric expressions in Equations (14) and (15) do satisfy the conservative requirement of the conservation expression for first derivatives in general co-ordinates [8], e.g.

$$x_{\xi\eta} = x_{\eta\xi} \tag{17}$$

2.4. Discretization of the momentum equation

A momentum balance for control volume ($u^1_{i,j}$ is placed in the centre of this volume) gives:

$$\int_S \rho \mathbf{u}\mathbf{u} \cdot \mathbf{n}\, \mathrm{d}s = \int_S \mathbf{T} \cdot \mathbf{n}\, \mathrm{d}s \tag{18}$$

$\mathbf{T}$ is the stress tensor, $\mathbf{T} = \mathbf{S} - p\mathbf{I}$, $\mathbf{S}$ is the extra stress tensor

$$\mathbf{S} = \frac{2}{Re}[\mathbf{D} - \tfrac{1}{3}(\nabla \cdot \mathbf{u})\mathbf{I}] \tag{19}$$

$\mathbf{D}$ the rate of deformation tensor, in incompressible flow

$$S_{xx} = \frac{2}{Re} u_x, \quad S_{xy} = S_{yx} \frac{1}{Re}(u_y + v_x), \quad S_{yy} = \frac{2}{Re} v_y \tag{20}$$

The algebraic formulae for $\mathrm{d}s_e$ and $\mathrm{d}s_n$ are:

$$(uU)\,\mathrm{d}\eta|_e + \cdots = \frac{1}{Re}\left(C_1 u_\xi + C_2 u_\eta + \frac{y_\eta}{J}(U_\xi + V_\eta) + v_\eta\right)\mathrm{d}\eta|_e - p y_\eta\, \mathrm{d}\eta|_e + \cdots \tag{21}$$

$$(uV)\,\mathrm{d}\xi|_n + \cdots = \frac{1}{Re}\left(C_3 u_\eta + C_4 u_\xi - \frac{y_\xi}{J}(U_\xi + V_\eta) - v_\xi\right)\mathrm{d}\xi|_n + p y_\xi\, \mathrm{d}\xi|_n + \cdots \tag{22}$$

where

$$C_1 = J^{-1} g_{22}, \quad C_3 = J^{-1} g_{11}, \quad C_2 = C_4 = J^{-1} g_{12} \tag{23}$$

This relationship gives the equilibrium state for the control volume. Let us consider the terms of the right-hand sides of Equations (21) and (22), and some aspects of their approximations on the double staggered grids. For an orthogonal grid, $g_{12} = 0$, and $C_2 = C_4 = 0$. In the discretized form of Equations (21) and (22) terms $U_\xi + V_\eta$ are recognized as continuity equations in general curvilinear co-ordinates (Equations (7) and (11)) and disappear in the differential form (e.g. Reference [4]), terms v_ξ and v_η also vanish under conditions $\mathrm{d}\xi \to 0$, $\mathrm{d}\eta \to 0$, but if weak approximations are used for the integral form of Equation (18), there may arise situations in which there are additional friction components

$$\begin{aligned} &\frac{1}{Re}(-u_\eta\, \mathrm{d}\xi|_n + u_\eta v_\xi\, \mathrm{d}\xi|_s - u_\xi\, \mathrm{d}\eta|_e + u_\xi\, \mathrm{d}\eta|_w), \\ &\frac{1}{Re}(v_\xi\, \mathrm{d}\xi|_n - v_\xi\, \mathrm{d}\xi|_s = v_\eta\, \mathrm{d}\eta|_e - v_\eta\, \mathrm{d}\eta|_w) \end{aligned} \tag{24}$$

that vanish $\mathrm{d}\xi \to 0$ and $\mathrm{d}\eta \to 0$.

Rewrite (22) for the first grid, using explicit manner for u^1

$$(u^1 V^1)\,\mathrm{d}\xi|_n + \cdots = \frac{1}{Re}\left(C_3 u^1_\eta + C_4 u_\xi - \frac{y_\xi}{J}(U^1_\xi + V^1_\eta) - v_\xi\right)\mathrm{d}\xi|_n + p y_\xi\,\mathrm{d}\xi|_n + \cdots \tag{25}$$

here U^1 and V^1 are expressed in terms of double grid variables (Equations (8) and (9)). In a similar manner, design equation for u^1 may be derived from the second grid

$$u^1_\xi|_n = (u^2_{i+1,j+1} - u^2_{i,j+1})/\mathrm{d}\xi \tag{26}$$

Thus, this double grid gives an advantage over displacement routines when, in place of u_η averages of u^1 are used

$$v^1_\xi|_n = (v^1_{i+1,j+1} - v^1_{i+1,j})/\mathrm{d}\xi, \quad p = p^2_{i+1,j+1} \tag{27}$$

In (25) each derivative is discretized in terms of the two neighbouring points, based on the assumptions of linear profiles, and is evaluated in terms of the values from the previous iteration.

A particular scheme for discretization of the left-hand sides of Equations (21) and (22) depends on the relative importance of convection and diffusion. Central differencing can be used for a suitably small mesh size. For fluid flow problems in general, convection may be large and, therefore, the scheme should account for the special influence of the upstream points. Convection and diffusion flux on the control volume surface are combined to define the total flux J_e on surface e

$$J_e = F_e u^1 + D_e u^1_\xi + S_e \tag{28}$$

where the flow rate, F_e, the diffusion coefficients, D_e and the additional diffusion source, S_e are given by

$$F_e = (U\,\mathrm{d}_\eta)|_e, \quad D_e = \left.\left(\frac{C_1}{Re}\,\mathrm{d}\eta\right)\right|_e, \quad S_e = \frac{1}{Re}(C_2 u^1_\eta - v_\eta)\,\mathrm{d}\eta|_e \tag{29}$$

For an orthogonal grid and on condition that the terms of Equation (24) are equal to zero, $S_e = 0$, and Equation (29) fully coincides in form with the one-dimensional case.

In the present paper, we use approximation schemes [1]. In general, for any J_e

$$J_e - F_e u^1_P = a_E(u^1_P - u^1_E) \tag{30}$$

where P and E are neighbouring points, and

$$a_E = D_e A\left|\frac{F_e}{D_e}\right| + \max|-F_e, 0| \tag{31}$$

Two different functions are used for A in examples.

The final form of the discretized momentum equation specific to grid point $u^1_{i,j}$ may be written as (a more detailed treatment of a single staggered grid was presented by

Patankar [1])

$$a^{1u}_{i,j}u^1_{i,j} = a^{1u}_{i+1,j}u^1_{i+1,j} + a^{1u}_{i-1,j}u^1_{i-1,j} + a^{1u}_{i,j+1}u^1_{i,j+1} + a^{1u}_{i,j-1}u^1_{i,j-1} - (p^1_{i,j} - p^1_{i-1,j})y_\eta \,\mathrm{d}\eta + (p^2_{i,j+1} - p^2_{i,j})y_\xi \,\mathrm{d}\xi + S^1_{i,j} \tag{32}$$

where a is similar to Equation (31), a and S include second grid approximation.

From Figure 1(b) it is evident that all the above discussion for u^1 may be applied to component v^2 of the secondary field. In internal grid points the a-coefficients should be the same. The following explanations cover certain cases in which the control volume is connected to the boundary.

1. If the e-point lies on the body surface, then non-slip conditions $u^1 = 0$, $v^2 = 0$ are applied.
2. If the e-point lies on the symmetry axes, $u^1_\xi = 0$, $v^2 = 0$, and the a-coefficients are different.

Thus, a differential approximation for the boundary cells depends on the boundary conditions on the cell side, and two types of the boundary conditions may be specified for the same cell side, e.g. Dirichlet conditions for the second v^2 component, and Neuman condition for the u^1 component

$$v^2 = 0, \quad u^1_\xi = 0 \tag{33}$$

3. VELOCITY–PRESSURE LINKAGE

3.1. Pressure correction equation

The method used here for handling the velocity–pressure linkage resembles the SIMPLE procedure [1] for Cartesian co-ordinates. In this method, the guessed pressure field is used to obtain a flow field from the momentum equation. This flow field does not satisfy the continuity equation at the first iteration, therefore, the pressure field is corrected so that the resulting velocity field satisfies the continuity equation. The pressure correction equation is derived by combining the continuity equation with truncated forms of the momentum equation. After the pressure correction equation has been solved, the velocity and pressure fields are corrected, and the procedure is repeated until the numerical solutions converge.

In a general co-ordinate system the pressure correction equation contains two derivatives p_η and p_ξ. In deriving the pressure correction equation, Shyy *et al.* [2] dropped the p_η term or the p_ξ terms to retain the structure of the five-point approximation in each finite-difference equation. This permits retention of the simple and efficient tri-diagonal equation solver. An alternative formulation [2–4] is to put the p_η term and p_ξ term into the source term in the pressure–correction equation.

Other techniques for the SIMPLE algorithm will be generalized to general co-ordinates with a double staggered grid. Let us assume that a guessed pressure field p^{1^*}, the solution to the momentum equation (Equation (32)) was obtained. Then it is assumed that the correction of the pressure is given by

$$p^1 = p^{1^*} + p^{1'} \tag{34}$$

which yields new solutions

$$u^1 = u^{1^*} + u^{1'}, \quad v^1 = v^{1^*} + v^{1'}, \quad u^2 = u^{2^*} + u^{2'}, \quad v^2 = v^{2^*} + v^{2'} \tag{35}$$

With Equations (34) and (35), and the procedure for staggered grid [1], we can obtain the correction equations for first field velocity, terms involving second pressure are inputted to the source in the momentum equations:

$$u^1_{i,j} = u^{1^*}_{i,j} - (p^{1'}_{i,j} - p^{1'}_{i-1,j}) y_\eta / a^{1u}_{i,j} \tag{36}$$

$$v^1_{i,j} = v^{1^*}_{i,j} - (p^{1'}_{i,j} - p^{1'}_{i,j-1}) x_\xi / a^{1v}_{i,j} \tag{37}$$

$$u^2_{i,j} = u^{2^*}_{i,j} + (p^{1'}_{i,j} - p^{1'}_{i,j-1}) y_\xi / a^{2u}_{i,j} \tag{38}$$

$$v^2_{i,j} = v^{2^*}_{i,j} + (p^{1'}_{i,j} - p^{1'}_{i-1,j}) x_\eta / a^{2v}_{i,j} \tag{39}$$

With these results (Equations (36)–(39)) the correction equation for contravariant velocity components can be obtained

$$U^1_{i,j} = u^{1^*}_{i,j} y_\eta - v^{2^*}_{i,j} x_\eta - (p^{1'}_{i,j} - p^{1'}_{i-1,j}) g_{22} / a^{1u}_{i,j} \tag{40}$$

$$V^1_{i,j} = v^{1^*}_{i,j} x_\xi - u^{2^*}_{i,j} y_\xi - (p^{1'}_{i,j} - p^{1'}_{i,j-1}) g_{11} / a^{1v}_{i,j} \tag{41}$$

Equations (40) and (41) are substituted into the continuity equation (Equation (7)) and the pressure correction equation is given by

$$a_{i,j} p^{1'}_{i,j} = a_{i,j+1} p^{1'}_{i,j+1} + a_{i,j-1} p^{1'}_{i,j-1} + a_{i-1,j} p^{1'}_{i+1,j} + a_{i-1,j} p^{1'}_{i-1,j} + S_{i,j} \tag{42}$$

In a similar manner, the design equation (Equation (42)) may be derived for the second pressure, on the assumption that the first pressure is entered into the source of the momentum equation.

The solution of the Poisson equation in the discretized form (Equation (42)) yields p', which is added to p^*, giving an updated value for p. This updated pressure is used to replace p^* in successive cycles of iteration.

3.2. Pressure boundary conditions

The use of the algorithm SIMPLE in combination with domain discretization by means of the MAC mesh allows the computation of the first pressure p^1 without requiring the explicit specification of boundary conditions. At the boundaries, non-centred first-order or second-order derivatives are used when necessary.

Two examples of how to specify boundary conditions for both pressures fields and how to couple them at the boundary are described below for external flow (cylinder) and forced convection within a cavity.

3.3. Generalization of the SIMPLE algorithm to a double grid

The overall computational procedure that was adopted is identical to the well-known SIMPLE algorithm of Patankar [1]. The procedure is iterative, to account for the coupling of velocity

and pressure, and the non-linearity in the momentum equations. Each iteration involves, in sequence:

At the intermediate iterations, known field values of the first and second primitive variables: p^{1^*}, $\mathbf{u}^{1^*}$, p^{2^*}, $\mathbf{u}^{2^*}$,

- calculating **a** coefficients for u^1;
- checking boundary conditions, and if necessary, calculating only the values of the boundary **a**-coefficients for v^2;
- iterating the momentum equation with the pressures p^{1^*}, p^{2^*} to obtain the new velocity field component u^{1^*};
- calculating **a**-coefficients for v^1;
- checking boundary conditions, and if necessary, calculating only the values of the boundary **a**-coefficients for u^2;
- iterating the momentum equation with the pressures p^{1^*}, p^{2^*} to obtain the new velocity field component v^{1^*};
- calculating U, V contravariant velocity components, and Poisson equation coefficients for pressure correction $p^{1'}$;
- iterating the Poisson equation for pressure correction $p^{1'}$;
- correcting the first pressure field and velocity field, calculating the boundary conditions to pressure fields;
- calculating coefficients for the second velocity field $\mathbf{u}^2$ in accordance with the new field variables;
- iterating the momentum equation with the new pressure p^{1^*}, to obtain the new velocity field component u^{2^*};
- iterating the momentum equation with the new pressures p^{1^*}, to obtain the new velocity field component v^{2^*};
- calculating the Poisson equation coefficients for pressure correction $p^{2'}$;
- iterating the Poisson equation for pressure correction $p^{2'}$;
- correcting the second pressure field and the second velocity field;
- repeat the cycle from the beginning as necessary:

$$\| p^{n+1} - p^n \| < \varepsilon_p \tag{43}$$

The successive line under-relaxation (SLUR) method was used to solve the Poisson equations for pressure correction and for momentum equation components. The relaxation parameter depends on the properties of the algebraic equation systems and ranges up to 1.0.

4. ADAPTATION OF THE SOLUTION METHODOLOGY

The use of the methodology will be illustrated by means of numerical studies of external flow over a circular cylinder and internal driven flow in a cavity.

4.1. Viscous incompressible flow over a circular cylinder

The problem of viscous incompressible flow over a circular cylinder has a long history and numerous theoretical and numerical solutions have been developed by Fornberg [9],

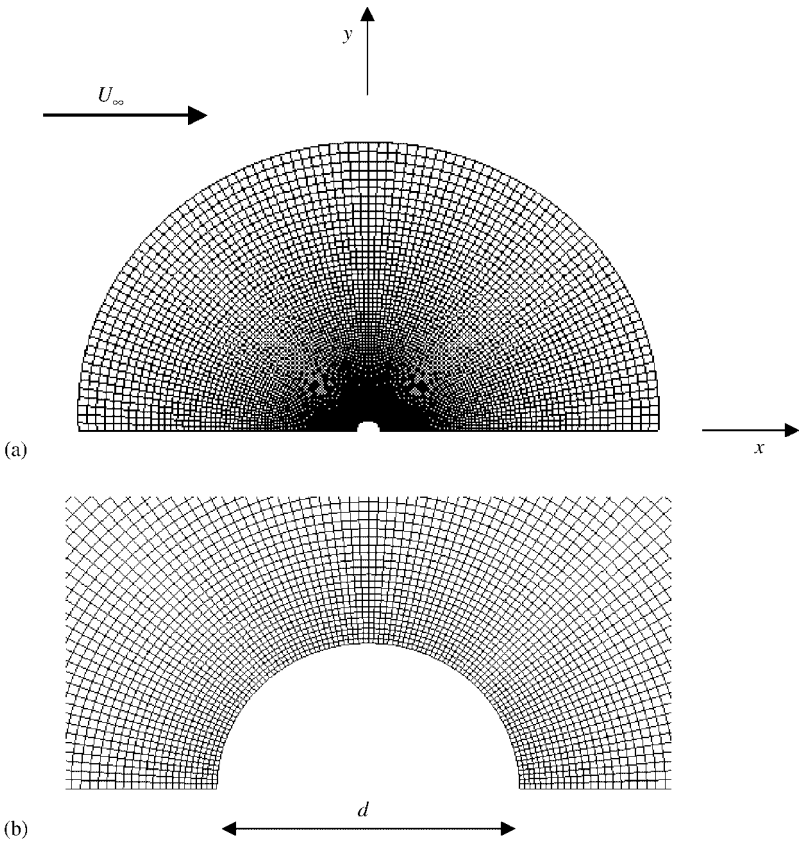

Figure 2. (a) Circular cylinder computational physical domain; (b) grid at the cylinder surface.

Imai [10], Braza *et al.* [11] and others (see Reference [12]). This example problem is concerned with flow over a circular cylinder. The Reynolds number Re, based on the diameter d, is $Re_d = U_\infty d/v$. The quantity U_∞ is the free-stream velocity and v is the kinematic coefficient of viscosity.

The x, y domain and conform grid 100×100 are presented at the Figure 2, ratio of the domain radius to cylinder radius is 50.

Something of the aspect of the definitions of the boundary conditions on the double staggered grid discussed above formed the basis of this special case—flow over a cylinder. Far-field conditions were carefully considered [9] in terms of stream function ψ and vorticity ω. Four different choices of boundary condition for ψ were considered:

- free stream (using $\psi = 0$ on the outer edge);
- one term of the Oseen approximation (see, e.g. Reference [10]);
- normal derivative zero ($\psi_\xi = 0$);
- and, 'mixed conditions' connecting ψ and ψ_ξ on the boundary.

From careful consideration of all these conditions, it appears that the use of the $\psi_\xi = 0$ for Reynolds numbers up to about 40 solves the problem of boundary conditions for ψ at large

distances. Thus, in definitions

$$u = \psi_y + 1, \quad v = -\psi_x \tag{44}$$

in co-ordinates ξ, η at the boundary

$$u_\Gamma y_\xi - v_\Gamma x_\xi = y_\xi \tag{45}$$

or

$$V_\Gamma = -y_\xi, \quad U_\Gamma = (Ju_\Gamma + y_\xi x_\eta)/x_\xi \tag{46}$$

For computational procedures it is preferable to write

$$v_\Gamma = (u_\Gamma - 1) y_\xi / x_\xi \tag{47}$$

in potential flow $u_\Gamma = 1$ and 0.

Additional infinite boundary conditions for this elliptic system must be defined. An upwind approximation of the vorticity transport may be added, but with a loss of accuracy [10]. In the present paper, the condition $\omega_\xi = 0$ was used at the boundary.

In our discussion, we have adhered to control volume definitions, therefore, from the continuity equation

$$u_\Gamma = \frac{1}{J}(U_e + V_n - V_s) x_\xi - \frac{y_\xi x_\eta}{J} \tag{48}$$

Pressure normal derivatives to x-axis:

$$p_y = (-x_\eta p_\xi + x_\xi p_\eta)/J \tag{49}$$

for $x_\eta = 0$, and Equation (49) is equivalent to

$$p_\eta = 0 \tag{50}$$

and this Neumann condition for pressure is discretized by one-sided differences

$$p_0 = \tfrac{9}{8} p_1 - \tfrac{1}{8} p_2 \tag{51}$$

At the cylinder surface, the η-axis coincides with the cylinder, and no-slip conditions are applied for the grid functions $\mathbf{u}^1, \mathbf{u}^2$.

The Neumann conditions for the wall pressure p^1 are obtained from the differential form of the momentum equation at the cylinder surface. The symbol w denotes cylinder surface nodes and, therefore, $w - \frac{1}{2}$—denotes the centre of the first grid mesh adjacent to this surface,

$$\frac{C_1}{ReJ} u_{\xi\xi}\bigg|_w = y_\eta p_\xi|_w - y_\xi p_\eta|_w, \quad \frac{C_1}{ReJ} v_{\xi\xi}\bigg|_w = -x_\eta p_\xi|_w + x_\xi p_\eta|_w \tag{52}$$

on the orthogonal grid

$$p_\xi|_w = \frac{1}{ReJ}(y_\eta u_{\xi\xi}|_w - x_\eta v_{\xi\xi}|_w) \tag{53}$$

$$p_\eta|_w = \frac{C_1}{ReJ^2}(x_\eta u_{\xi\xi}|_w + y_\eta v_{\xi\xi}|_w) \tag{54}$$

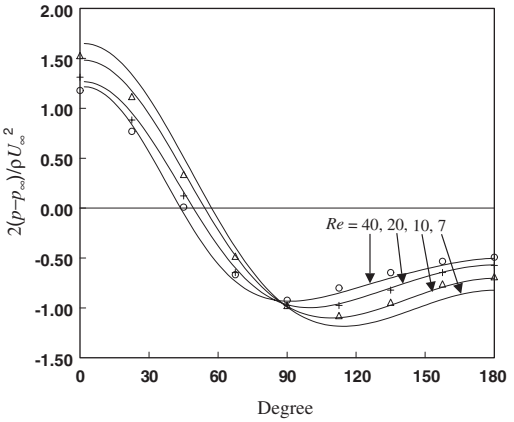

Figure 3. Pressure coefficient on the cylinder surface: present study: —, $Re = 7, 10, 20, 40$. Fornberg [9]: ○, $Re = 40$; +, 20; Δ, 10.

From Equations (53) and (54), explicit surface coupling between p^1 and p^2 may be found

$$p^2_{w,j+1/2} = p^1_{w,j} + p^1_\eta|_{w,j}\, \mathrm{d}\eta/2 \tag{55}$$

where

$$p^1_{w,j} = p^1_{w-1/2,j} + p^1_\eta|_{w-1/2,j}\, \mathrm{d}\xi/2 \tag{56}$$

Power-law scheme [1] are used in Equation (30) to approximate both convection and diffusion fluxes

$$A\left|\frac{F}{D}\right| = \max\left|0, \left(1 - 0.1\left|\frac{F}{D}\right|\right)^5\right| \tag{57}$$

Calculations were performed with grids ranging from 40×40 to 100×100, with double precision on PC with an accuracy of 10^{-15}. No attempt was made to optimize the code in order to reduce run times for this problem, or for the other solutions described below.

Figure 3 shows the distribution of the wall pressure coefficients, compared with the numerical results of Fornberg [10]. The calculation of the wall pressures at the rear and the front of the cylinder are given in Table I.

In Figure 4 the dimensionless negative vorticity on the surface of the cylinder is shown. Agreement with the numerical results of Braza *et al.* [11] was found to be satisfactory.

Various characteristic quantities, including $C_f, C_p, \theta_s, l_w/d$ are listed in Tables II and III. The separation angle, θ_s (listed in Table III) was determined from the condition $\omega = 0$ at the surface of the cylinder. The results for $Re \leqslant 40$ have generally been computed from a steady-state model; maximum and minimum results [12] are presented in the tables, although in some cases only one value is tabulated. The agreements between present and tabulated values are seen to be reasonably good.

Table I. Present calculations and published values (cited by Churchill [11]) for the pressure coefficients at the rear and the front of the cylinder.

	$2(p_0 - p_\infty)/\rho u_\infty^2$			$2(p_r - p_\infty)/\rho u_\infty^2$		
Re_d	Max	Min	Present	Max	Min	Present
10	0.742	0.670	0.702	1.500	1.474	1.481
20	0.589	0.537	0.565	1.274	1.261	1.271
30	0.556	0.530	0.539	1.184	1.176	1.178
40	0.555	0.509	0.519	1.144	1.117	1.138

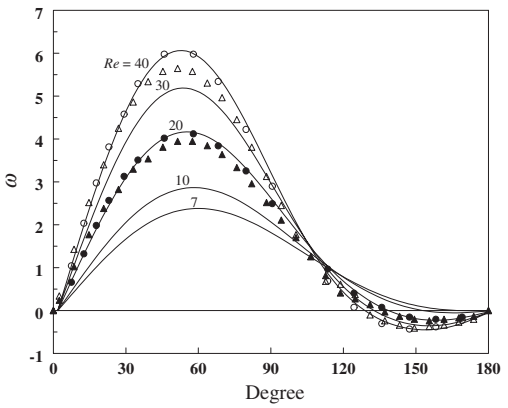

Figure 4. Vorticity distribution over the surface of the cylinder: present study: —, $Re = 7, 10, 20, 30, 40$. Braza *et al.* [11]: ○, $Re = 40$; ●, 20. Fornberg [9]: Δ, $Re = 40$; ▲, 20.

Table II. Present calculations and published values (cited by Churchill [11]) for friction drag coefficients and pressure drag coefficients.

	C_f			C_p		
Re_d	Max	Min	Present	Max	Min	Present
10	0.623	0.615	0.610	0.800	—	0.789
20	0.427	0.406	0.393	0.662	0.617	0.617
30	0.332	—	0.309	0.508	—	0.548
40	0.284	0.257	0.259	0.538	0.498	0.511

4.2. Lid-driven cavity flow

The second test case involves laminar flows in which the fluid motion is induced by the movement of one wall (lid-driven cavity flows), as shown in Figure 5. Appropriate benchmark solutions were described by the Demirdžić *et al.* [13]. Non-orthogonal grids were set up by inclining the sidewalls or by squeezing the cavity. Test case Cl corresponds to the angle $\beta = 45°$, and test case C2 corresponds to $\beta = 30°$. In both cases, $L = 1$, density $\rho = 1$, and lid velocity $U_L = 1$ were used in the calculations. The Reynolds number, defined for a lid velocity, $U_L = 1$, and cavity length, L, was varied from 100 to 1000.

Table III. Present calculations and published values (cited by Churchill [11]) for attachment angle and wake length.

	l_w/d			θ_s		
Re_d	Max	Min	Present	Max	Min	Present
10	0.530	0.434	0.499	29.3	28.00	28.8
20	1.880	1.683	1.827	43.7	42.80	43.1
30	3.223	2.855	3.159	49.6	49.07	49.09
40	4.690	4.046	4.488	54.2	50.00	53.02

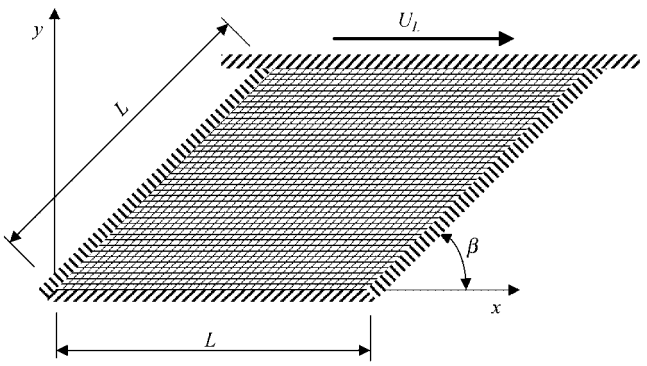

Figure 5. Geometry, boundary conditions and uniform grid for test cases.

Non-uniform, symmetrically expanding towards the centreline from all walls, were implied by Demirdžić *et al.* [13], e.g. on the finest grid, with a 320×320 control volume, the smallest Δx was $L/757$.

Uniform grids from 160×160 to 480×480 are used for testing double staggered algorithms. For the type of grid as shown in Figure 5, $x_\xi = 1$, $y_\xi = 0$, $x_\eta = \cos\beta$, $y_\eta = \sin\beta$. Boundary conditions are $v = u = 0$ at the walls and the bottom, and $v = 0$, $u = U_L$ at the cavity top. Central-differences are used in Equation (31) to approximate both convection and diffusion fluxes [1]

$$A\left|\frac{F}{D}\right| = 1 - 0.5\left|\frac{F}{D}\right| \tag{58}$$

In the momentum equations, values of the pressure at the boundary nodes are required to evaluate the pressure gradient. Linear extrapolation from interior values of the pressure was used for collocated grids [13]. Comparisons between the presented algorithm and bench-mark solutions were done by linear extrapolation from interior values, e.g. at the bottom wall

$$p_0^1 = 0.5(3p_1^1 - p_2^1) \tag{59}$$

p^2 at the walls is computed as the average of p^1; this method of calculating the wall pressure is valid for a small field gradient at the wall, but in the general case the wall pressure must be determined by means of the momentum equation.

The Neumann conditions for the wall pressure p obtained from the differential form of the momentum equation at the walls (for grid type in Figure 4) at the left and right

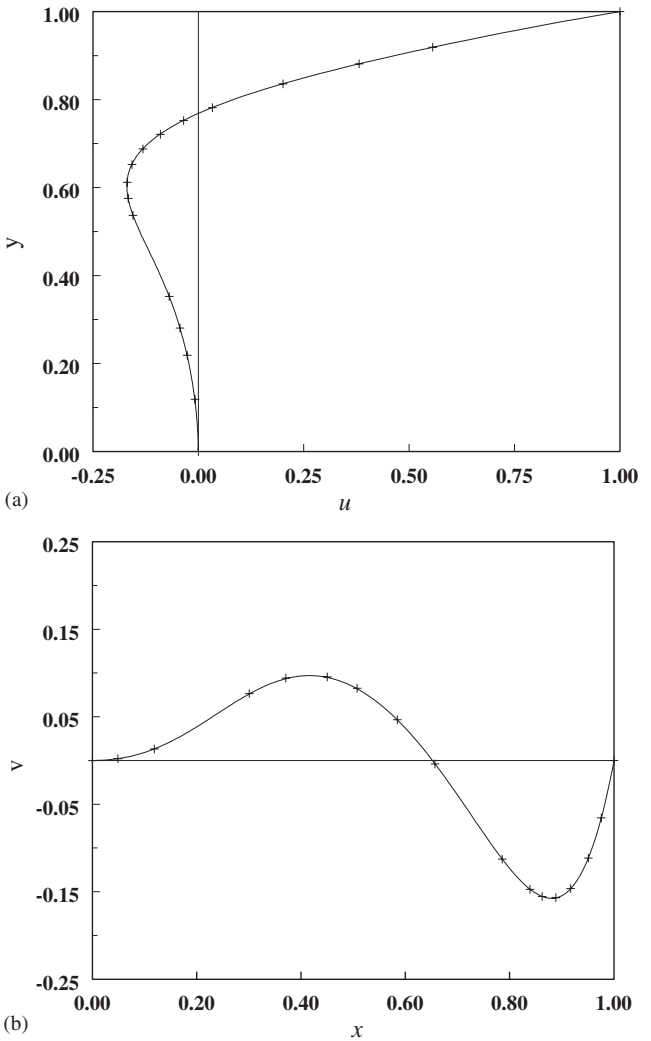

Figure 6. Centreline velocity profiles for $Re = 100$, $\beta = 45^\circ$; (a) u-component; (b) v-component: —, present study; +, Demirdžić *et al.* [13].

walls $(\xi = 0, 1)$

$$p_\xi = (u_{\xi\xi} - 2x_\eta u_{\eta\xi})\frac{1}{Re\, y_\eta^2} + v_{\xi\xi}\frac{1}{Re} - (Uu)_\xi \frac{1}{y_\eta} + (U_\xi + V_\eta)_\xi \frac{1}{Re} \tag{60}$$

at these walls p_ξ is used for calculations of p^1, and p_η for calculation of p^2 along this walls

$$p_\eta = (x_\eta u_{\xi\xi} - 2x_\eta^2 u_{\eta\xi} + y_\eta v_{\xi\xi} - 2x_\eta y_\eta v_{\eta\xi})\frac{1}{Re\, y_\eta^2} - (Uu)_\xi \frac{x_\eta}{y_\eta} - (Uv)_\xi \tag{61}$$

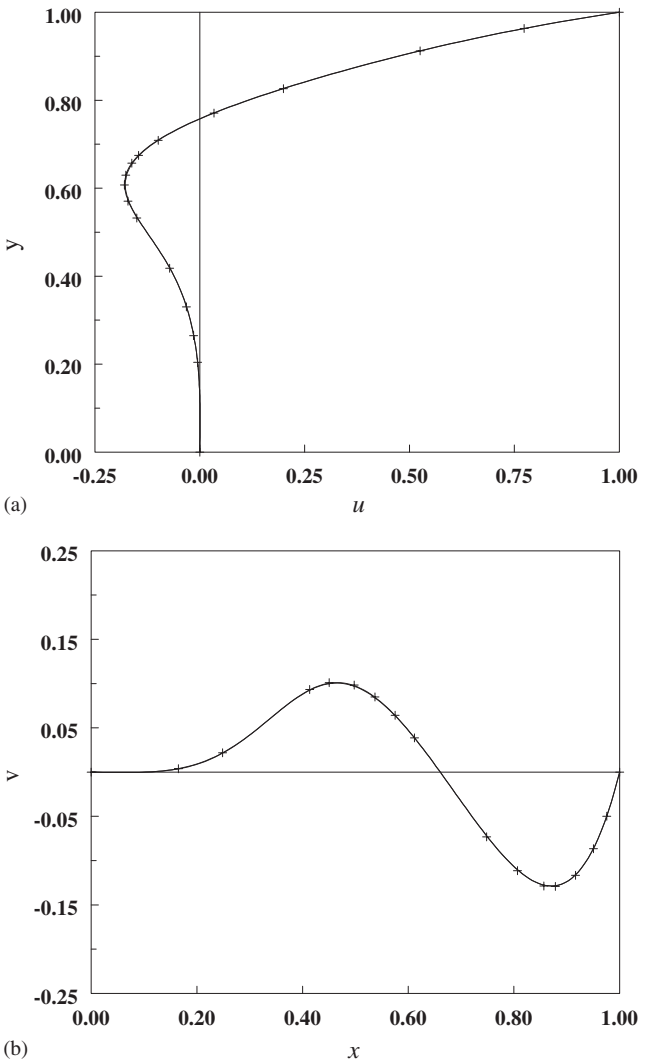

Figure 7. Centreline velocity profiles for $Re = 100$, $\beta = 30^\circ$; (a) u-component; (b) v-component: —, this study; +, Demirdžić *et al.* [13].

and at the top and bottom walls ($\eta = 0, 1$)

$$p_\eta = (x_\eta u_{\eta\eta} - 2x_\eta u_{\eta\xi} + y_\eta v_{\eta\eta} - 2y_\eta v_{\eta\xi})\frac{1}{Re\, y_\eta^2} - (Vu)_\eta \frac{x_\eta}{y_\eta} - (Vv)_\eta \tag{62}$$

$$p_\xi = (u_{\eta\eta} - 2x_\eta u_{\eta\xi})\frac{1}{Re\, y_\eta^2} - (Vu)_\eta \frac{1}{y_\eta} \tag{63}$$

at these walls p_η is used for calculation of p^1 at the walls, and p_ξ for calculation of p^2. Pressures at the walls are calculated in accordance Equations (55) and (56). Extrapolated

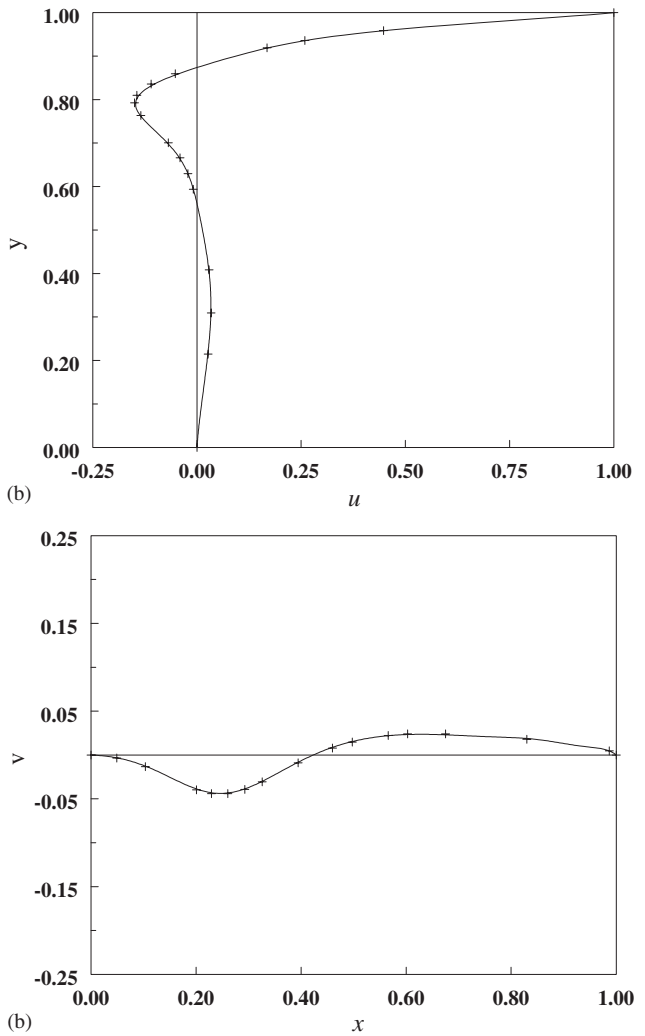

Figure 8. Centreline velocity profiles for $Re = 1000$, $\beta = 45°$; (a) u-component; (b) v-component: —, present study; +, Demirdžić *et al.* [13].

values p^1 or p^2 are corrected in accordance to the maximum (minimum) theorem for elliptic equations. p^1 should be more (less) than its neighbours at the cell boundaries.

The double staggered algorithm was tested with double precision on a Workstation Alpha XP 1000. The iteration number of the pressure correction equation was found to be 10 and that of the momentum equation was set to 4. For $Re = 100$, Figures 6 and 7 show excellent agreement with bench-mark solutions [13]. For $Re = 1000$ the results of the double staggered grid and the collocated multi-grid method [13] were in quite close agreement, as seen in Figures 8 and 9, these figures also show that the u velocity components are in slight disagreement at their maximum. Streamlines predicted on the 320×320 grids for flow case $\beta = 30°$

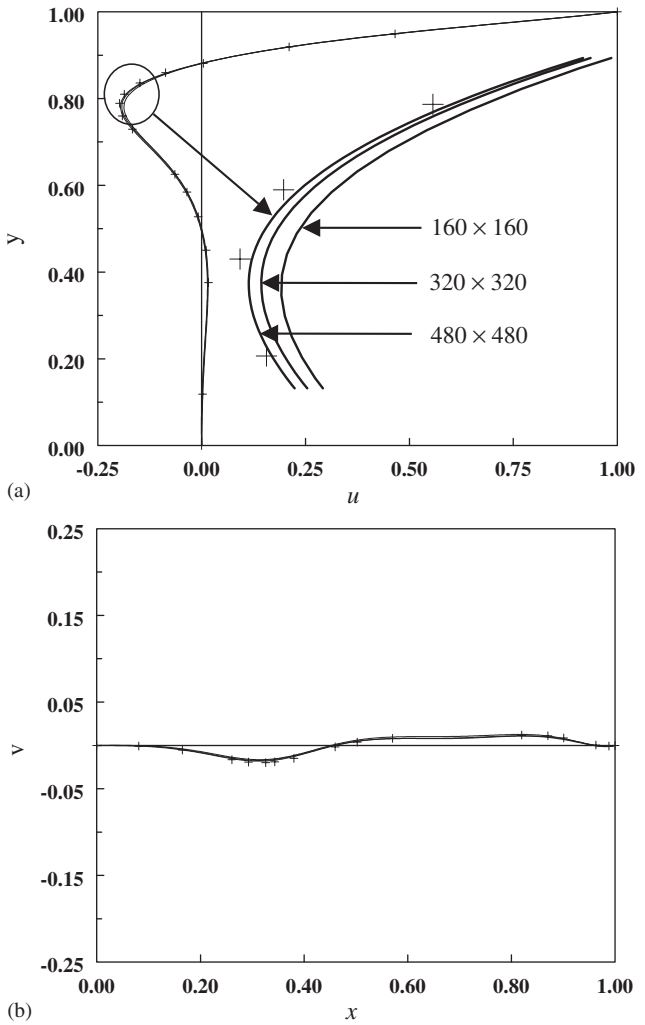

Figure 9. Centreline velocity profiles for $Re = 1000$, $\beta = 30°$; (a) u-component; (b) v-component: —, present study; +, Demirdžić *et al.* [13].

and $Re = 1000$ are presented in Figure 10; they show typical features of such flow [13]. The pattern of the streamlines was calculated from the vorticity-stream function formulation of one of the momentum equations (see Reference [14]).

$$\Delta\Psi + \omega = 0 \tag{64}$$

or, for grid type at Figure 5

$$C_1\Psi_{\xi\xi} + C_3\Psi_{\eta\eta} - 2C_2\Psi_{\xi\eta} + x_\eta u_\eta + y_\eta v_\xi - u_\eta = 0 \tag{65}$$

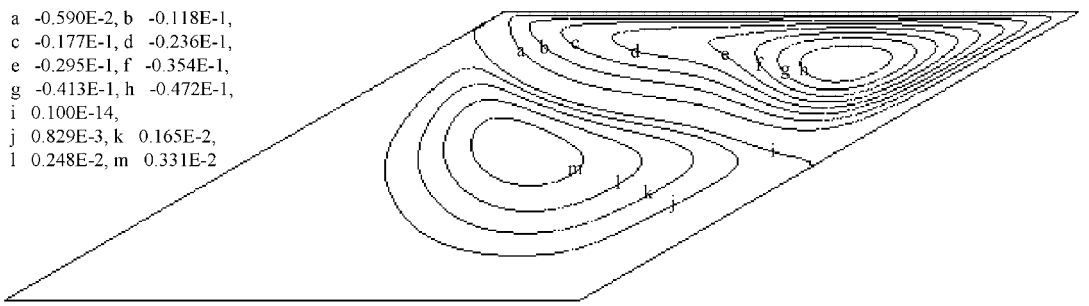

Figure 10. Predicted streamlines for $Re = 1000$, $\beta = 30°$.

Table IV. Minimum and maximum stream function values in vortex centres, and their positions.

	$Re = 100$		$Re = 1000$	
	Demirdžić *et al.* [13]	Present	Demirdžić *et al.* [13]	Present
$\beta = 45°$				
$\Psi_{\min}$	-7.0226×10^{-2}	-7.0129×10^{-2}	-5.3507×10^{-2}	-5.2553×10^{-2}
x	1.1100×10^{-0}	1.1146×10^{-0}	1.3130×10^{-0}	1.3120×10^{-0}
y	5.4638×10^{-1}	5.4581×10^{-1}	5.7404×10^{-1}	5.7453×10^{-1}
ε	0.0219405	0.0219405	0.1068854	0.1068854
$\Psi_{\max}$	3.6831×10^{-5}	3.9227×10^{-5}	1.0039×10^{-2}	1.0039×10^{-2}
x	3.3867×10^{-1}	3.2075×10^{-1}	7.7663×10^{-1}	7.7663×10^{-1}
y	1.4308×10^{-1}	1.9888×10^{-1}	3.9851×10^{-1}	3.9851×10^{-1}
ε	1.3554620	1.3554620	0.3313280	0.3313280
$\beta = 30°$				
$\Psi_{\min}$	-5.3135×10^{-2}	-5.3004×10^{-2}	-3.8566×10^{-2}	-3.8185×10^{-2}
x	1.1664×10^{-0}	1.1674×10^{-0}	1.4583×10^{-0}	1.4583×10^{-0}
y	3.7898×10^{-1}	3.7813×10^{-1}	4.1086×10^{-1}	4.1093×10^{-1}
ε	0.0332841	0.0332841	0.0538782	0.0538782
$\Psi_{\max}$	5.6058×10^{-5}	5.7000×10^{-5}	4.1494×10^{-3}	3.8891×10^{-3}
x	5.2692×10^{-1}	5.2105×10^{-1}	9.0386×10^{-1}	8.9008×10^{-1}
y	1.4334×10^{-1}	1.5433×10^{-1}	2.5501×10^{-1}	2.6446×10^{-1}
ε	5.0257323	5.0257323	0.8776961	0.8776961

The double grid arrangement was also applied to (65); Neuman conditions $\Psi^1_{\xi}|_{\xi=0,1} = 0$, $\Psi^1_{\eta}|_{\eta=0} = 0, \Psi^1_{\eta}|_{\eta=1} = 1$ were set for the first grid function, Ψ^1, and wall boundary conditions were set to zero for the second grid function, Ψ^2. Minimum and maximum stream function values in vortex centres and their positions as predicted on the 320×320 grid are presented in Table IV. Small quantitative differences were found in the displacement of the maximum stream function values of the vortexes and its intensities.

5. CONCLUSIONS

A methodology has been presented for the numerical solution of two-dimensional convection–diffusion problems for arbitrary solution domains. Special features of the methodology include:

- Use of a double-staggered grid (DSG) in general curvilinear co-ordinates.
- Use of the integral form of the conservation equations as the starting point for the derivation of the finite-difference equations.
- Development of a new set of boundary conditions for primitive variables for an arbitrary domain.
- The discretized equations and their solutions were linked to the widely used SIMPLE algorithm for orthogonal systems.

Use of this methodology was illustrated by the solutions of external flow over a circular cylinder and lid-driven cavity internal flow. The numerical results were found to be in good agreement with published solutions.

The DSG method as presented can be extending to the solution of additional problems (heat transfer, turbulence quantities, etc.). The development of such an extension is presently under way.

NOMENCLATURE

$\mathbf{a}$	influence coefficients matrix in the finite difference equation
C	drag coefficient
C_1, C_2, C_3, C_4	transformed diffusion coefficients
J	Jacobian of the transformation
J	mass flux
$\mathbf{g}$	matrix transformation
l	length
p	pressure
Re	Reynolds number
S	source term in the discretized equations
$\mathbf{u}$	velocity vector
u, v	Cartesian velocity components
U, V	contravariant velocity components
x, y	Cartesian co-ordinate system
ξ, η	general curvilinear co-ordinates
θ	angle
ρ	density
φ	general scalar field
ψ	stream function
ω	vorticity, $\omega = v_x - u_y$

Superscripts

1,2	first and second primitive variables fields
*	tentative variables fields

$'$	field correction
u	velocity

Subscripts

E, P, N, S, W	values associated with centres of neighbour control volumes
e, n, s, w	values associated with control volumes faces
f	friction
p	pressure
r	rear stagnation point
s	separation angle
x, y, ξ, η	partial derivatives
w	wake
Γ	domain boundary
0	front stagnation point
∞	free stream

REFERENCES

1. Patankar SV. *Numerical Heat Transfer and Fluid Flow*. Hemisphere: New York, 1980.
2. Shyy W, Tong SS, Correa SM. Numerical recirculating flow calculation using a body-fitted coordinate system. *Numerical Heat Transfer* 1985; **8**:99–113.
3. Faghri M, Sparrow EM, Prata AT. Finite-difference solutions of convection–diffusion problems in irregular domains, using a nonorthogonal coordinate transformation. *Numerical Heat Transfer* 1984; **7**:183–209.
4. Maliska CR, Raithby GD. A method for computing three dimensional flows using non-orthogonal boundary-fitted co-ordinates. *International Journal for Numerical Methods in Fluids* 1984; **4**:519–537.
5. Peyret R, Taylor TD. *Computational Methods for Fluid Flow*. Springer: New York, 1982.
6. Lien FS, Leschziner MA. A general non-orthogonal collocated finite volume algorithm for turbulent flow at all speeds incorporating second-moment turbulence-transport closure, Part 1: computational implementation. *Computer Methods in Applied Mechanics and Engineering* 1994; **114**:123–148.
7. Rhie CM, Chow WL. Numerical study of the turbulent flow past an airfoil with trailing edge separation. *AIAA Journal* 1983; **21**:1525–1532.
8. Thompson JF (ed.). *Numerical Grid Generation*. North-Holland: New York, 1982.
9. Fornberg B. A numerical study of steady viscous flow past a circular cylinder. *Journal of Fluid Mechanics* 1980; **98**:819–855.
10. Imai I. On the asymptotic behavior of viscous fluid flow at a great distance from a cylindrical body, with special reference to Filon's paradox. *Proceedings of the Royal Society Series A* 1951; **208**:487–516.
11. Braza M, Chassaing P, Minh H. Numerical study and physical analysis of the pressure and velocity fields in the near wake of a circular cylinder. *Journal of Fluid Mechanics* 1986; **165**:79–130.
12. Churchill SW. *Viscous Flows*. Butterworths: London, 1988.
13. Demirdžić I, Lilek Ž, Perić M. Fluid flow and heat transfer test problems for non-orthogonal grids: bench-mark solutions. *International Journal for Numerical Methods in Fluids* 1992; **15**:329–354.
14. Fletcher CAJ. *Computational Techniques for Fluid Dynamics*. Springer: Berlin, 1988.

